Nanoscale Advances



COMMUNICATION

View Article Online



Cite this: DOI: 10.1039/d5na00497g

Received 20th May 2025 Accepted 28th September 2025

DOI: 10.1039/d5na00497g

rsc.li/nanoscale-advances

Polydopamine and hyaluronic acid-coated dualresponsive silica nanoparticles for targeted atherosclerosis imaging and therapy

Yuanzhe Lin, ab Chenyuan Huang, ac Xiao Hou, ad James Chen Yong Kah*b and Jiong-Wei Wang acceptated

Atherosclerosis remains the primary cause underlying cardiovascular diseases, however, there is no plaque-targeting pharmacotherapy clinically available. Nebivolol (NB), a third-generation beta-blocker clinically used to treat hypertension and heart failure, exerts potent antioxidative activities by inhibiting reactive oxygen species (ROS) production and scavenging ROS. Here, we developed an atherosclerotic plague lesional macrophage-targeting nanotheranostic system that is coated with polydopamine (PDA) as a contrast agent to facilitate non-invasive photoacoustic imaging (PAI) of atherosclerotic plaques and NB as a drug to eliminate plague ROS. In brief, mesoporous silica nanoparticles (MSNs) with interpenetrating chiral channels were coated with bioinspired PDA polymers (SPDA). PDA on the nanoparticle surface was then conjugated with hyaluronic acid (HA) to allow active targeting to atherosclerotic macrophages that overexpress CD44 (SPDA@HA). Upon loading of NB, the resulting NB/SPDA@HA nanoparticles could eliminate ROS and alleviate inflammation in activated macrophages. In addition, NB/SPDA@HA nanoparticles inhibited cell apoptosis and oxidized low density lipoprotein induced foam cell formation. Moreover, the silanols on the silica surface and the HA coating on the MSNs enable accelerated drug release from NB/SPDA@HA nanoparticles in response to the acidic and hyaluronidase-rich microenvironment in the plaque. Taken together, the dual-responsive NB/SPDA@HA nanotheranostic platform represents a promising nanomedicine for targeted atherosclerosis imaging and therapy.

Introduction

Atherosclerosis is the main cause of adverse cardiovascular events such as myocardial infarction and stroke, which

accounted for 32% of global deaths in 2019.¹ Atherosclerosis development is generally asymptomatic until the occurrence of vessel blockage or plaque rupture. Therefore, early diagnosis is important for atherosclerosis management. However, clinical strategies are subject to many limitations. Magnetic resonance imaging (MRI) has limited sensitivity and is prone to produce artifacts due to vascular pulse² while intravascular ultrasound (IVUS) is invasive and prone to induce complications including irregular heart rhythms, deep vein thrombosis and allergic reaction.³ Photoacoustic imaging (PAI) is an emerging noninvasive imaging modality that enables the conversion of absorbed near-infrared light (NIR) light to ultrasonic signals with high spatial resolution, high contrast and deep tissue penetration,⁴ making it a promising modality for imaging atherosclerosis.

Atherosclerosis is characterized by build-up of lipid-laden and macrophage-rich plaques on the arterial wall. Increased reactive oxygen species (ROS) production from M1 macrophages induces inflammation within atherosclerotic plaques. 5,6 In addition, ROS exacerbate the progression of atherogenesis by oxidizing low density lipoprotein (LDL), prompting overexpression of adhesion molecules and scavenger receptors, and inducing apoptosis of endothelial cells, vascular smooth muscle cells and macrophages.^{5,6} Unfortunately, anti-ROS strategies, including oral administration of probucol, proanthocyanidin, methotrexate, darapladib and torcetrapib, generated inconsistent or marginal therapeutic outcomes, largely due to low accumulation of anti-ROS drugs within the plaque.7 This poses a significant challenge for clinical translation. However, delivery of antioxidant compounds with nanoparticles has been shown to remarkably increase intraplaque drug concentrations, resulting in improved treatment efficacy of atherosclerosis.8-11 Yet, most of those drug delivery systems rely on passive targeting attributable to the enhanced permeability and retention effect present in the inflaming plaques. On the other hand, drug delivery efficiency may be improved by employing ligandmediated active targeting of nanoparticles to the plaque.12

While numerous nanoparticles have been designed for atherosclerosis management, their clinical potential is

^aDepartment of Surgery, Yong Loo Lin School of Medicine, National University of Singapore, 119228 Singapore, Singapore. E-mail: surwang@nus.edu.sg

^bDepartment of Biomedical Engineering, National University of Singapore, 117583 Singapore, Singapore. E-mail: kah@nus.edu.sg

^cCardiovascular Research Institute (CVRI), National University Heart Centre Singapore (NUHCS), 117599 Singapore, Singapore

^dNanomedicine Translational Research Program, Yong Loo Lin School of Medicine, National University of Singapore, 117609 Singapore, Singapore

^eDepartment of Physiology, Yong Loo Lin School of Medicine, National University of Singapore, 117593 Singapore, Singapore

hindered by low drug loading capacity and limited biocompatibility. Mesoporous silica nanoparticles (MSNs) have garnered significant interest in biomedical applications due to their unique physical properties, which include large surface area and pore volume, controllable particle size, facile surface modification and excellent biocompatibility.13 To our knowledge, the use of MSN-based nanomedicine for plaque specific drug delivery and diagnosis remains relatively unexplored.

Here, we coated MSNs with bioinspired polydopamine (PDA) polymers¹⁴ (MSN-PDA, referred to as SPDA hereinafter) that exert efficient NIR absorption and excellent PAI conversion efficiency to synthesize SPDA nanoparticles, enabling PAI (Scheme 1). Hyaluronic acid (HA), a natural ligand for CD44 receptor that is prominently expressed on lesional macrophages within atherosclerotic plagues, 15-17 was further functionalized on SPDA (SPDA@HA) to allow active targeting to M1 macrophages within atherosclerotic plagues. As ROS in atherosclerotic lesions are mainly generated by endothelial nitric oxide synthase (eNOS) uncoupling and nicotinamide adenine dinucleotide phosphate (NADPH) oxidase,18 both of which can be inhibited by Nebivolol (NB), a third-generation beta-blocker clinically used to treat hypertension and heart failure, 19,20 we loaded NB into SPDA@HA to obtain NB/SPDA@HA nanoparticles. Since CD44 is overexpressed in plaque lesional macrophages, NB could be delivered specifically to atherosclerotic plaques by NB/SPDA@HA nanoparticles. Moreover, the abundant hyaluronidase (HAase) in the plaque21 can break down the HA coating and the intraplague mild acidic microenvironment²² can reduce the electronic interactions between NB and silanols on the MSNs, resulting in an accelerated release of NB from the nanoparticles. Therefore, our NB/SPDA@HA nanoparticles may represent a highly desirable nanotheranostic platform for targeted atherosclerosis therapy.

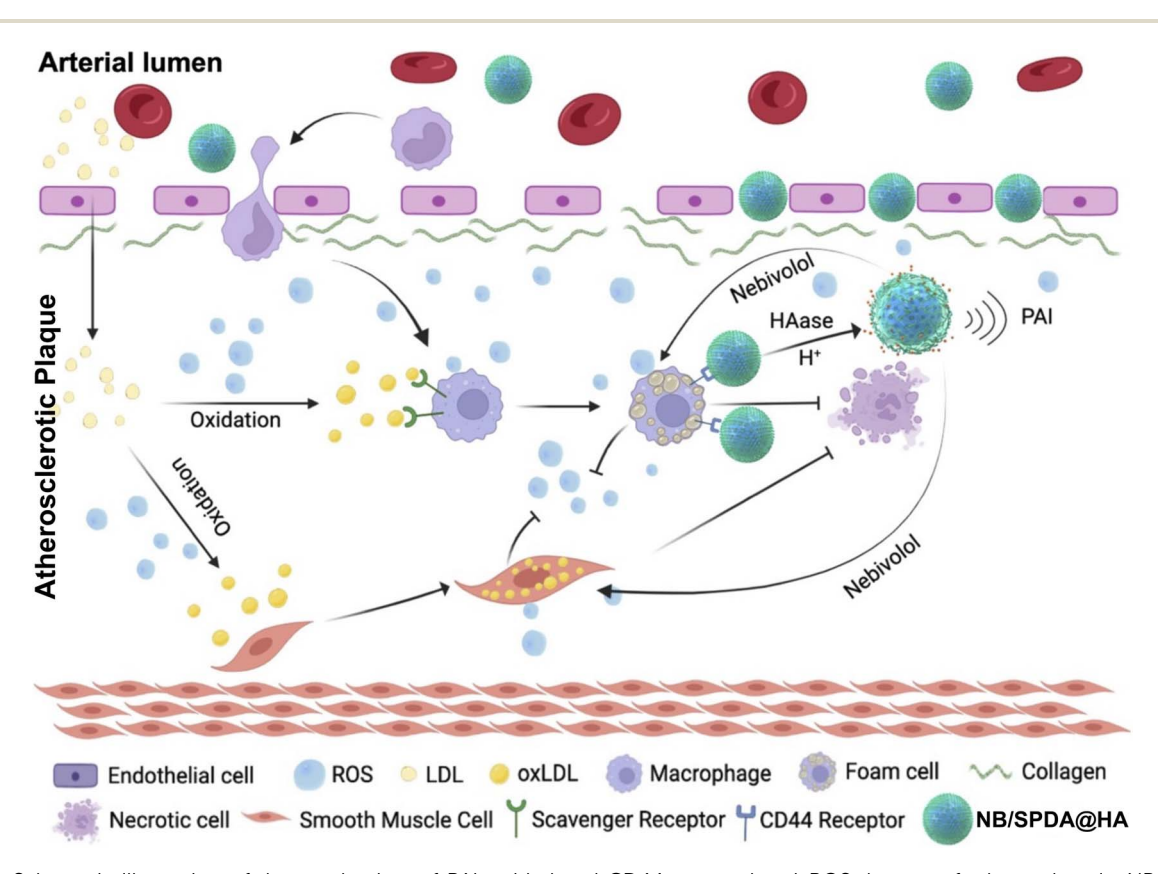
Materials and methods

Materials

Tetraethyl orthosilicate (TEOS), cetrimonium bromide (CTAB), Pluronic F-127, dopamine hydrochloride (DA), hyaluronic acid (HA), and NH₄OH were purchased from Sigma-Aldrich (USA). Cy5 was purchased from Lumiprobe (USA). PrestoBlue, DAPI, anti-CD44 antibody and IFN-γ were purchased from Invitrogen (USA). DMEM, FBS, penicillin, streptomycin and HEPES were purchased from Gibco (USA). IL-6, IL-1β and TNF-α ELISA kits were purchased from Biolegend (USA). DCFH-DA kit and oxidized low density lipoprotein (oxLDL) were purchased from Thermo Fisher (USA). FITC-Annexin V & propidium iodide apoptosis detection kit was purchased from BD bioscience (USA).

Synthesis of NB/SPDA@HA nanoparticles

The mesoporous silica nanoparticles (MSNs) were synthesized as previously described with minor adaptions. Briefly, 0.5 g



Scheme 1 Schematic illustration of the mechanism of PAI-guided and CD44-targeted anti-ROS therapy of atherosclerosis. NB/SPDA@HA releases loaded Nebivolol (NB) in response to plaque microenvironment (acidic pH, high hyaluronidase), leading to local reduction of ROS and inflammation. This process is further guided and monitored using photoacoustic imaging (PAI) for precise localization. This targeted approach is designed to both monitor and attenuate atherosclerosis progression in a plaque-targeted manner.

CTAB and 6 g triblock copolymer F127 were dissolved in 96 ml Milli-Q water, in which 43 ml absolute ethanol and 11 ml 29 wt% ammonium hydroxide solution were added. Afterwards, 1.8 g TEOS were introduced into the mixture dropwise under vigorous stirring, and the mixture was kept still at room temperature for 24 h. The synthesized nanoparticles were collected at 10 000 rpm and resuspended into 100 ml absolute ethanol containing $\mathrm{NH_4NO_3}$ under reflux at 80 °C for 24 h to extract the template. In the end, MSNs were washed 3 times and

Communication

kept in methanol for further use.

Nebivolol (NB) was loaded into MSNs by solvent evaporation method. In brief, MSNs were dispersed in methanol solution containing NB (0.25 mg ml $^{-1}$) and stirred overnight at 500 rpm and 40 °C in the dark. Thereafter, obtained NB/MSN was washed with a mixture of methanol and water thrice. Free NB was determined at $\lambda=283$ nm and subtracted from the total amount of NB to determine drug loading. Cy5 was labelled on SPDA@HA following the same procedure as NB loading for subsequent cell uptake studies.

PDA was coated on the surface of MSNs through the solution oxidation method. In brief, MSNs and dopamine hydrochloride (DA) were added into pH 8.5 Tris-HCl buffer with a mass ratio of 2:1 and stirred overnight. The synthesized MSN-PDA (SPDA) was collected at 9000 rpm and washed with Milli-Q water thrice. Hyaluronic acid (HA) was then conjugated to SPDA through $\rm Fe^{3+}$ -mediated coordination reaction²³ where 30 mg SPDA was redispersed in Tris-HCl buffer (pH 8.5) followed by addition of 100 $\rm \mu I\ FeCl_3\ (6\ mg\ ml^{-1})$ solution and continuous stir for 1 h to form the final drug-loaded NB/SPDA@HA or its non-drug loaded SPDA@HA counterpart.

The drug loading (DL) capacity was calculated according to the following formula:

$$DL\% = m_2/(m_1 + m_0) \times 100\%$$

 m_0 , m_1 and m_2 represent the total mass of SPDA@HA added to the reaction system, the total mass of NB put in the reaction system and the loaded mass of NB, respectively.

Characterization of NB/SPDA@HA nanoparticles

The morphology and size of SPDA@HA were characterized by transmission electron microscopy (TEM) (JEOL 2200FS Cryo TEM, JEOL USA, Inc.) and dynamic light scattering (DLS) (Nanosizer, Malvern Instruments Ltd, Worcestershire, UK), respectively. The specific surface area and pore size distribution were measured by ASAP® 2425 instrument (Micromeritics, USA) based on Brunauer–Emmett–Teller (BET) theory. NB/SPDA@HA composition was determined by thermogravimetric analysis (TGA) (METTLER TOLEDO, USA) and Fourier-transform infrared spectroscopy (FT-IR) (INVENIO, Bruker, USA).

For the *in vitro* photoacoustic imaging (PAI) phantom study, different concentrations of SPDA@HA nanoparticles were injected into the capillary and scanned with a high resolution PAI tomography scanner (Vevo LAZR-X, FUJIPILM, Japan).

Mouse macrophages (RAW264.7) were seeded in a black 96-well plate at a density of 10^4 cells/well in 100 μ l comprehensive

DMEM (cDMEM) to evaluate the cytotoxicity of SPDA@HA nanoparticles. Cells were treated with various concentrations of SPDA@HA over a range of time interval and cell viability was measured with PrestoBlue assay (ThermoFisher).

To evaluate dual-responsiveness of the nanoparticles to pH values and HAase enzyme, 5 mg NB/MSN and NB/SPDA@HA were dispersed into 15 ml release buffers at 37 °C: (1) pH 5.0 PBS, (2) pH 7.4 PBS, (3) pH 5.0 PBS + 150 U ml⁻¹ HAase, (4) pH 7.4 PBS + 150 U ml⁻¹ HAase. An equal volume of release medium was collected at indicated time intervals after centrifugation for measuring the released NB with UV-Vis absorption spectrophotometry at 283 nm.

Cellular uptake of SPDA@HA in vitro

CD44 receptor expression was first determined on inflammatory RAW264.7 macrophages [macrophage cell line derived from male BALB/c mice, American Type Culture Collection (ATCC) no. TIB71]. Briefly, cells were treated with LPS (300 ng ml $^{-1}$) and IFN- γ (20 ng ml $^{-1}$) (LPS/IFN- γ treatment) in cDMEM medium overnight to generate the M1 phenotype, whereas naïve macrophage group was cultured in cDMEM only. Cells were then stained with FITC-conjugated anti-CD44 antibody for FACS analysis, triplicates for each group.

RAW264.7 cells (naïve or M1 macrophages) were incubated with various concentrations of Cy5/SPDA and Cy5/SPDA@HA in FBS-free DMEM medium for 2 h at 37 °C or 4 °C to examine for targeting or passive binding of the nanoparticles, respectively. A competitive binding experiment was also conducted to further examine the role of CD44 in mediating nanoparticle uptake. In brief, LPS/IFN- γ -treated cells were incubated with 2 mg ml⁻¹ HA for 2 h and incubated with 25 μ g ml⁻¹ Cy5/SPDA@HA for another 2 h. The cells were then detached and washed thrice prior to FACS analysis of intracellular Cy5 MFI (mean fluorescence intensity).

For microscopic analysis, RAW264.7 cells were seeded into 12-well plates at 10^5 cells/well. Both M1 and naïve macrophages were incubated with 25 μg ml $^{-1}$ Cy5/SPDA@HA for 2 h. Competitive binding experiment was also performed as described above. After incubation with cold PBS, cells were rinsed thrice and fixed with 4% paraformaldehyde followed by nuclus staining with DAPI (4',6-diamidino-2-phenylindole). Images were taken under an inverted fluorescence microscope (ECLIPSE Ti, NIKON, Japan).

ROS-scavenging, anti-inflammatory and anti-apoptosis effects of NB/SPDA@HA *in vitro*

RAW264.7 cells were seeded into 12-well plates at 5×10^5 cells/well and incubated overnight. Naïve macrophages were treated with fresh cDMEM and M1 macrophages were generated by incubation with LPS/IFN- γ for 4 h. Macrophages were treated with NB/SPDA@HA (NB at 18 μ M) in the presence of LPS/IFN- γ . Subsequently, cells were stained with DCFH-DA kit at 37 °C and then detect intracellular ROS was examined by FACS and fluorescence microscopy. Cell culture supernatant was collected to measure inflammatory cytokines, including IL-6, IL-1 β and TNF- α , with ELISA kits.

To evaluate the impact of NB/SPDA@HA on cell apoptosis, native or M1 RAW264.7 macrophages incubated with various formulations for 24 h were stained with FITC-Annexin V and propidium iodide and then analyzed with FACS.

Effect of NB/SPDA@HA nanoparticles on foam cell formation

RAW264.7 cells cultured in cDMEM in the absence (naïve macrophages) or presence (M1 macrophages) of LPS/IFN-γ were incubated with NB drug formulations for 24 h, followed by incubation with 50 µg ml⁻¹ oxidized low-density lipoprotein (oxLDL) for another 48 h. Cells were washed twice with 0.5 M HCl in 70% ethanol and fixed with 10% formalin. Fixed cells were stained with Oil red O (ORO) solution as previously described9 and washed with 60% isopropanol for optical microscopy. To quantify intracellular cholesterol, intracellular

ORO was extracted with absolute isopropanol and measured by UV-Vis spectrophotometry at 492 nm.

Results and discussion

Synthesis and characterization of NB/SPDA@HA nanoparticles

The synthesis procedures of MSNs and NB/SPDA@HA were illustrated in Fig. 1A. MSNs were monodispersed with a diameter of 80 nm and mesopores that enable drug loading and subsequent drug release were clearly observed on the surface of MSNs (Fig. 1B). In this study, a third-generation beta-blocker Nebivolol (NB) that has been suggested to alleviate oxidative stress in atherosclerosis19,25,26 was loaded within the interconnected mesopores (Fig. 1A).

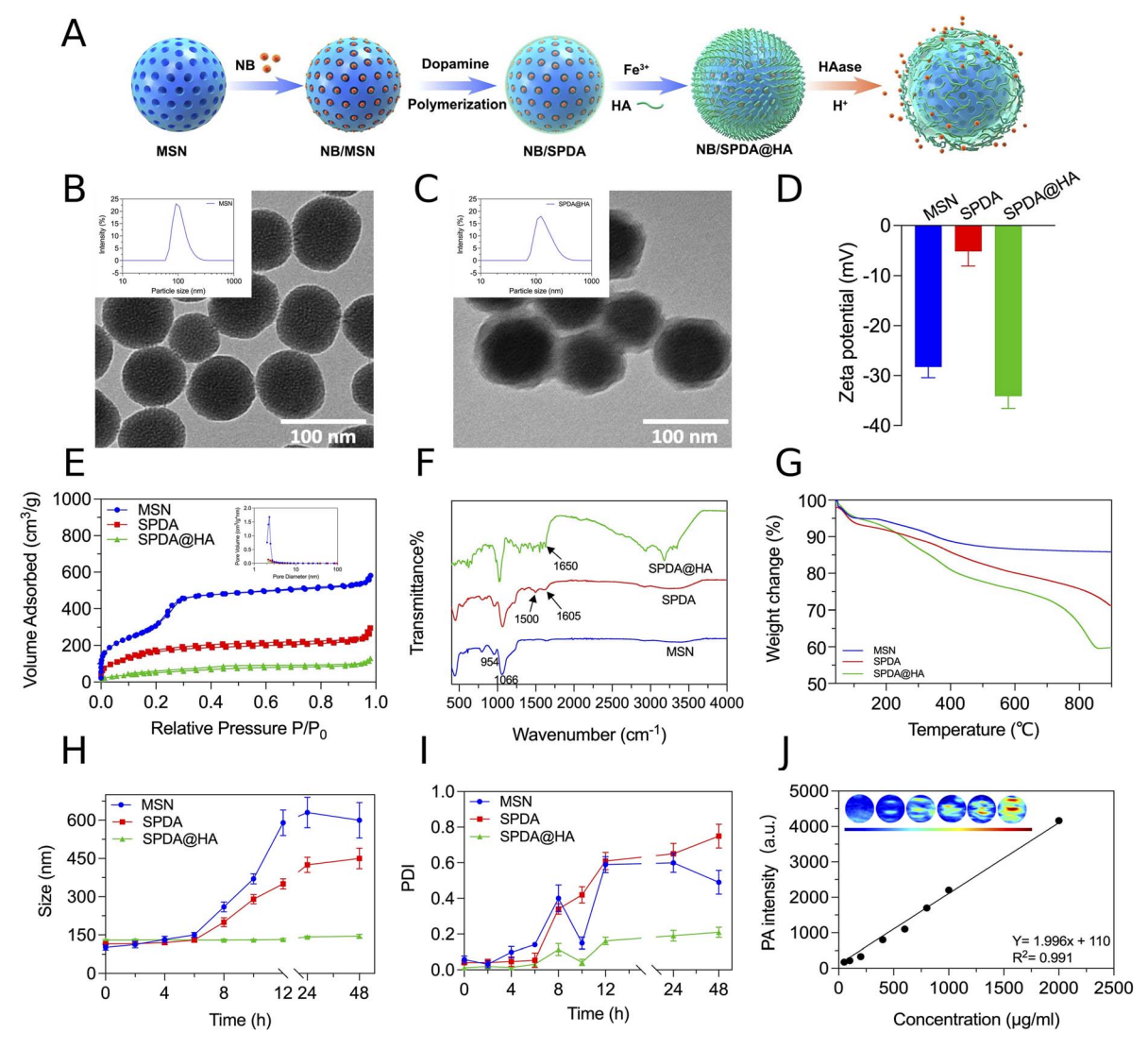


Fig. 1 Characterization of SPDA@HA nanoparticles. (A) The schematic illustration of SPDA@HA synthesis and loading of NB. (B and C) TEM images of (B) MSNs and SPDA@HA (C). (D) Zeta potentials of MSNs, SPDA and SPDA@HA. (E) The nitrogen adsorption/desorption isotherm with pore size distribution curves shown in the insert. (F) FT-IR spectrum of MSNs, SPDA and SPDA@HA nanoparticles. (G) Weight loss of MSN, SPDA and SPDA@HA nanoparticles determined by thermal gravimetric analysis (TGA). (H) Hydrodynamic diameter (D_n) and (I) polydispersity index (PDI) of MSN, SPDA and SPDA@HA. (J) Representative PAI images of SPDA@HA and its intensity calibration at different concentrations. Data is presented as mean \pm SD of three independent experiments in triplicates (D-J).

Communication Nanoscale Advances

To reduce premature leakage of NB and enable active targeting, MSNs were coated with PDA and HA to obtain NB/ SPDA@HA nanoparticles. PDA is structurally similar to melanin, possessing intense NIR light absorption and high PAI conversion efficiency. Additionally, PDA contains numerous functional groups, including catechol, amine and imine, which can serve as potential anchor points for different functional molecules.²⁷ HA is found abundantly in connective, epithelial, and neural tissues, and serves as the natural binding ligand for CD44 receptors, which are commonly overexpressed in macrophages within the plaque microenvironment. 16,17 This polymer modification resulted in a shell of approximately 10 nm thick (Fig. 1C, and S1). The Zeta potential (Fig. 1D) of MSNs was -28.3 mV due to the presence of abundant silanol groups on the surface.¹³ It became less negative at -5.2 mV after PDA modification, attributed to the formation of positively charged phenolic and amino groups during dopamine polymerization. 28,29 Following HA coating, the zeta potential became more negative again at -34.1 mV due to the presence of carboxyl groups within HA.30 The observed changes in zeta potential thus suggested a layered structure of NB/SPDA@HA nanoparticles, which was held together by strong electronic interactions.

The mesoporous structure of NB/SPDA@HA nanoparticles was analyzed by N2 adsorption/desorption assay. As shown in Fig. 1E and Table S1, the surface area (S_{BET}), total pore volume $(V_{\rm P})$ and pore size $(W_{\rm BIH})$ of MSNs was 1256 m² g⁻¹, 0.89 cm³ g⁻¹ and 2.3 nm, respectively, which were 5 to 10 times larger than that of other inorganic nanoparticles (e.g. Fe, Ag, Mo and Sn).31 The large surface area and pore volume are advantageous for drug loading. Furthermore, the gradually decreasing S_{BET} and $V_{\rm P}$ after each step of polymer coating indicate successful closing of mesopores by surface modifications.

To validate modifications by PDA and HA, Fourier transform infrared (FT-IR) spectroscopy was carried out. MSNs, SPDA and SPDA@HA all exhibited peaks at 1066 and 954 cm⁻¹ (Fig. 1F), ascribing to Si-O-Si stretching vibration and silanol group vibration, respectively. Following PDA coating, new peaks at 1500 and 1605 cm⁻¹ corresponding to the vibration of secondary amines and primary amine respectively were observed. Another distinctive adsorption peak was detected at 1650 cm⁻¹ following HA coating, which could be attributed to the carboxyl group (C=O) in HA.

Thermal gravimetric analysis (TGA) was used to quantify the amount of modified polymer through determining the gradual weight change over temperature. The weight change of MSNs, SPDA and SPDA@HA were 4.73%, 16.77% and 34.72%, respectively (Fig. 1G). A 12.04% weight loss from SPDA to MSNs could be attributed to the removal of PDA and a further 17.95% weight loss from SPDA@HA to SPDA might be resulted from removal of HA coating on the surface of SPDA. Collectively, these results indicate the mass composition of the modified polymers within SPDA@HA.

Colloidal stability of nanoparticles is critical in drug delivery applications. We hypothesized that the increased steric hindrance between nanoparticles due to HA coating could improve colloidal stability. Both MSNs and SPDA exhibited a significant increase in nanoparticle hydrodynamic diameter (D_h) and polydispersity index (PDI) following 6 h incubation in PBS (Fig. 1H and I, S1 and Table S2), indicating their loss of colloidal stability in biologically relevant media over time. In contrast, SPDA@HA exhibited exceptional stability up to 48 h incubation (Fig. 1H, I and S2).

PDA is structurally similar to naturally occurring melanin,³² possessing improved biocompatibility and biodegradability compared to other PAI contrast agents such as Au, Ag, Cu, Co. Our in vitro phantom study conducted using a photoacoustic tomography scanner showed that SPDA@HA could generate PAI signals (Fig. 1]), thus demonstrating its potential in improving the visualization of atherosclerotic plaques through PAI. Here, the PA signal intensity under 808 nm laser excitation showed a linear increase with the concentration of SPDA@HA nanoparticles (Fig. 1]). Importantly, SPDA@HA nanoparticles did not impose detectable cytotoxicity on RAW264.7 macrophages, primary macrophages derived from bone marrow or Hepa 1-6 hepatocytes at such concentrations (Fig. S3), suggesting their potential for drug delivery applications in vivo.

Drug loading and stimulation-responsive drug release

NB was loaded into MSNs followed by PDA and HA coating to form NB/SPDA@HA nanoparticles (Fig. 1A). At pH 7.4, the positively charged NB ($pK_a = 8.9$) interacted strongly with the negatively charged MSNs (Fig. 1D), resulting in a high drug loading of 32 wt% as determined by absorbance of NB at 283 nm (Fig. 2A). As expected, both NB/MSN and NB/SPDA@HA exhibited a characteristic absorption peak of NB at 283 nm which was not present in MSNs and SPDA@HA, indicating successful drug loading.

MSNs effectively addressed the poor solubility of NB by limiting the growth of drug particles.33 As shown in Fig. 2B, the pure NB exhibited distinct sharp Bragg peaks under X-ray diffraction (XRD) due to its crystalline nature. Upon loading of NB into the rigid pore structure of SPDA@HA, the majority of those sharp crystal diffraction peaks vanished (Fig. 2B), indicating a typical feature of amorphous silica and polydopamine.34,35 These data suggest that NB was dispersed and present in a non-crystalline physical state, resulting in enhanced solubility within SPDA@HA nanoparticles.

To release NB specifically within atherosclerotic plaques, NB/ SPDA@HA nanoparticles were designed to respond to both low pH and HAase enzyme. As shown in Fig. 2C, NB/MSNs exhibited rapid drug release at pH 5.6, reaching a cumulative release of NB up to 59.4% within 30 min, much faster than the release at pH 7.4. This phenomenon is attributable to the silanol group $(pK_a \text{ of } 5.6)$ on the silica surface. The surface charge at the silica-water interface is neutralized at pH 5.6,36 leading to disruption of the charge interaction between MSNs and NB and consequently release of NB. As macrophages in the plaques use glycolysis for ATP synthesis to fulfil their high energy demand under hypoxia, more lactate and protons were secreted,22 resulting in an acidic microenvironment. In fact, this acidic condition is commonly employed to design pH-responsive nanomedicine for accelerated drug release in the plaques. 10,37 Thus, one may expect that the pH-responsive feature of NB/

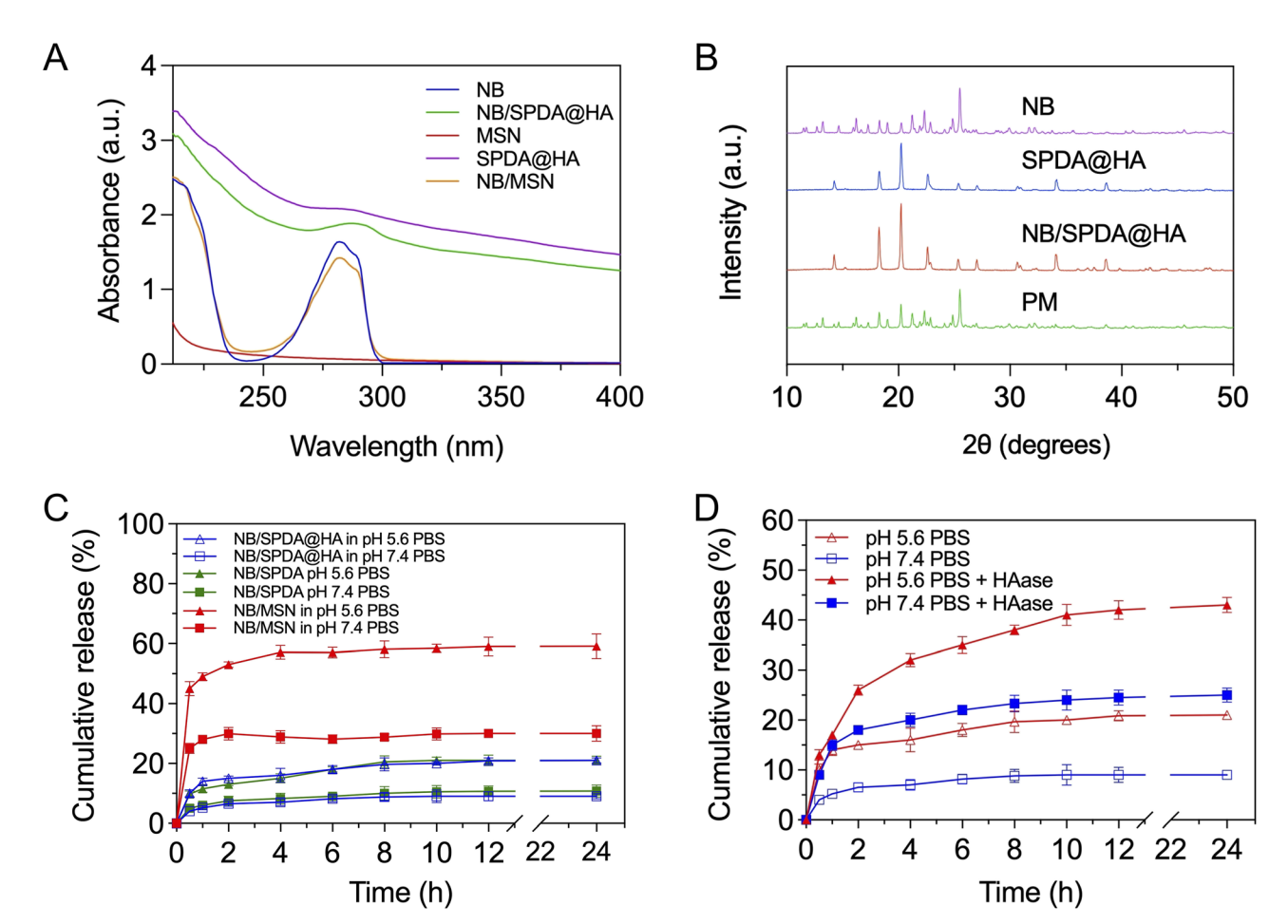


Fig. 2 Drug loading and drug release in vitro. (A) UV absorption spectrum of different samples with NB absorption peak at 283 nm. (B) X-ray diffraction (XRD) pattern of NB, SPDA@HA, NB/SPDA@HA and physical mixture (PM) of NB and SPDA@HA. (C) Cumulative release profiles of NB from NB/MSN, NB/SPDA and NB/SPDA@HA under pH 5.6 and pH 7.4. (D) Cumulative release profiles of NB from NB/SPDA@HA under different conditions. Data is presented as mean \pm SD of three independent experiments (C and D).

MSNs can enhance release of NB within atherosclerotic plaques, thereby improving therapeutic efficacy in atherosclerosis.

Interestingly, the pH-responsive NB release was also observed from NB/SPDA and NB/SPDA@HA nanoparticles albeit at a lower rate (Fig. 2C), likely due to restriction of drug diffusion by the PDA and HA bilayer polymer coated outside of the particles. This result indicates that the polymer coating could not completely restrain drug leakage as the drug concentration gradient outperforms the restriction posed by polymer coatings.³⁸ However, the coating was still effective in minimizing premature drug leakage before the carriers reached the target site. Furthermore, as the HA layer was readily degraded by HAase into small fragments, HAase increased the cumulative release of NB from NB/SPDA@HA regardless of pH values (Fig. 2D). Given that hyaluronidase (HAase) is highly abundant in atherosclerotic plaques,39 the HA coating facilitates both CD44-mediated targeting of NB/SPDA@HA nanoparticles and HAase-mediated accelerated drug release in the plaque. To further elucidate the release mechanism, we conducted comprehensive kinetic modeling of the release profiles using the Korsmeyer-Peppas equation (Fig. S4 and Table S3). The

results showed that Fickian diffusion was the predominant release mechanism for NB across all tested scenarios (with n consistently < 0.45). The presence of dual stimuli, the acidic pH and hyaluronidase, modulated both the release rate and mechanism, increasing the n value and shifting the profile toward more complex, anomalous transport. This indicates that matrix degradation and environmental responsiveness contribute to a more tunable and controlled release profile of NB/SPDA@HA. Taken together, NB/SPDA@HA represents a promising dual-responsive drug delivery system for atherosclerosis therapy.

Enhanced cellular uptake of SPDA@HA in vitro

As expected, M1 polarization induced by LPS/IFN-γ treatment significantly increased CD44 expression in RAW264.7 macrophages (Fig. 3A and S5). Since HA is the natural binding ligand of CD44 receptor,15-17 we examined if M1 polarization would enhance cellular uptake of nanoparticles by RAW264.7 cells. As shown in Fig. 3B, M1 RAW264.7 macrophages drastically enhanced cellular uptake of Cy5/SPDA@HA nanoparticles compared to naïve RAW264.7 cells in a dose-dependent Communication

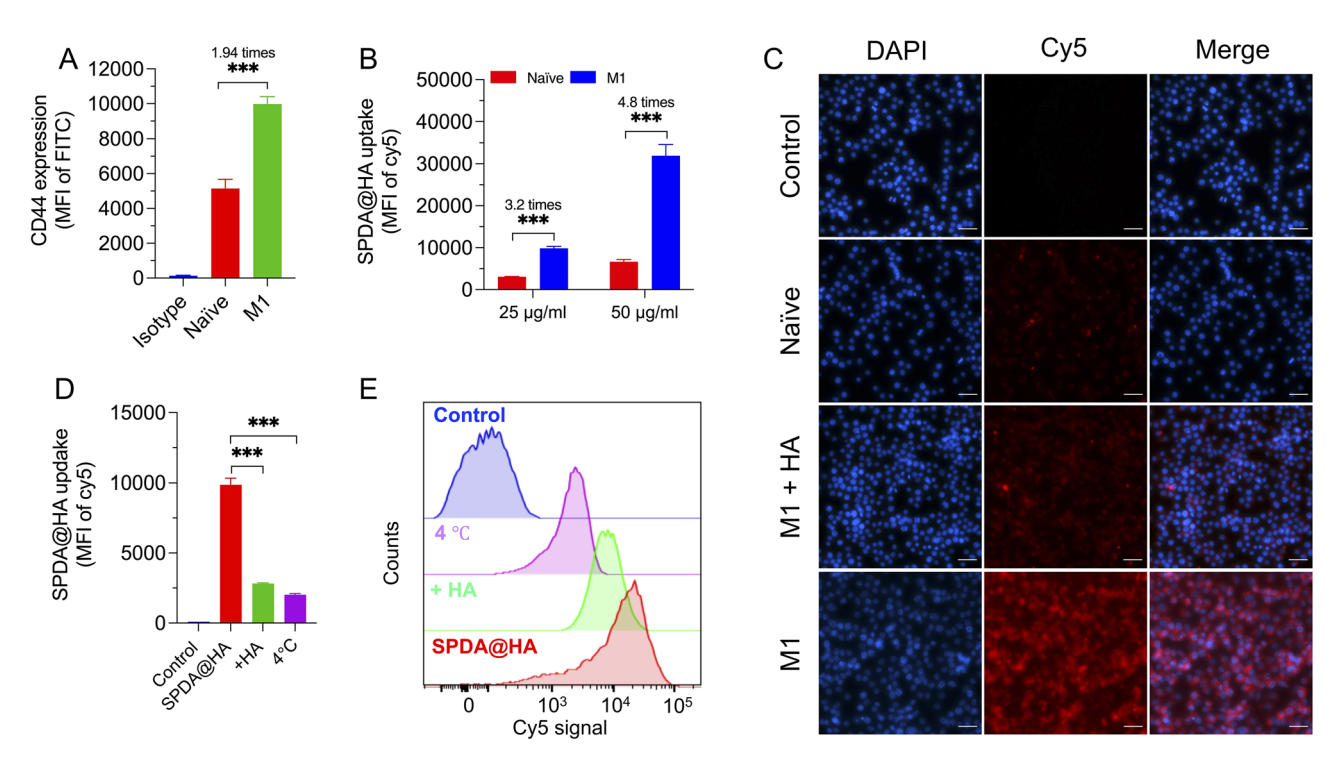


Fig. 3 Cellular uptake of SPDA@HA nanoparticles in vitro. (A) Quantification of CD44 expression in RAW264.7 cells by FACS. (B) Cellular uptake of Cy5/SPDA@HA by naïve and M1 RAW264.7 macrophages analyzed with FACS. Cells were incubated with 25 μg ml $^{-1}$ or 50 μg ml $^{-1}$ for 2 h at 37 °C followed by FACS. (C) Fluorescence microscopy images showing CD44 receptor-mediated uptake of Cy5/SPDA@HA nanoparticles by RAW 264.7 cells. Control, naïve macrophages without nanoparticles (blank control); Naïve, naïve macrophages incubated with Cy5/SPDA@HA; M1, M1 macrophages incubated with Cy5/SPDA@HA; M1 + HA, M1 macrophages incubated with Cy5/SPDA@HA in the presence of HA. Scale bar = 30 μm. (D and E) Quantification of cellular uptake of Cy5/SPDA@HA by M1 RAW264.7 macrophages in the absence (referred to as SPDA@HA) or presence (referred to as + HA) of HA at 37 °C or at 4 °C. M1 RAW264.7 macrophages without nanoparticles were used as blank control (referred to as control). Data is presented as mean \pm SD of three independent experiments. MFI, mean fluorescence intensity; ***p < 0.001.

manner. The enhanced cellular uptake of nanoparticles by macrophage M1 polarization was confirmed by fluorescence microscopy (Fig. 3C). Intriguingly, M1 RAW264.7 macrophages took up significantly more Cy5/SPDA@HA nanoparticles than Cy5/SPDA nanoparticles (Fig. S6), suggesting an involvement of CD44-HA mediated cellular uptake by M1 macrophages. To validate the enhanced uptake of SPDA@HA nanoparticles was mediated by CD44-HA interaction, we performed a ligandcompetitive binding experiment. As shown in Fig. 3C, pretreatment of M1 RAW264.7 macrophages with HA blocked cellular uptake of Cy5-labelled SPDA@HA nanoparticles. This result was confirmed by FACS analysis of mean fluorescence intensity of the cells pretreated with or without HA (Fig. 3D and E). These data indicate that HA pretreatment diminishes cellular uptake of uptake of SPDA@HA nanoparticles by blocking CD44 receptor binding sites to the HA coated on nanoparticles. Since receptor-mediated uptake involves ATPdependent endocytosis that is substantially affected by temperature,40 we examined cellular uptake of SPDA@HA nanoparticles at 4 °C (Fig. 3D and E). Compared to at 37 °C, cellular uptake activity of M1 RAW264.7 macrophages was markedly suppressed. These data further confirm that CD44 specifically mediates cellular uptake of SPDA@HA nanoparticles by macrophages. Since CD44 is highly expressed in lesional macrophages in atherosclerotic plaques, 15,17 HA coating

will therefore facilitate targeting and cellular uptake of SPDA@HA nanoparticles to achieve efficient delivery of NB to atherosclerotic lesions.

NB/SPDA@HA reduces intracellular ROS and suppresses inflammation in macrophages

We established a ROS-producing and inflammatory cell model by stimulating RAW264.7 macrophages with LPS/IFN-γ treatment to examine the anti-ROS activity of NB/SPDA@HA. Intracellular ROS was measured by incubating cells with a ROS fluorogenic probe, 2',7'-dichlorofluorescein diacetate (DCF-DA),41 which reacted with ROS to generate green fluorescence in the cells (Fig. 4A). After 4 h stimulation with LPS/IFN-γ, RAW264.7 macrophages produced considerably higher level of ROS, as determined by FACS (Fig. 4B and S7), than cells without stimulation. Intracellular ROS produced by LPS/IFN-γ was diminished by treatment with free NB, NB/SPDA and NB/ SPDA@HA nanoparticles (Fig. 4A and B and S7). NB/ SPDA@HA nanoparticles showed the most pronounced effects in ROS reduction, likely due to higher cellular uptake facilitated by HA coating (Fig. 3). The potent ROS reducing effect of NB in inflamed macrophages is likely due to its inhibition of ROS production and direct ROS-scavenging capability as previously reported. 19,20,25

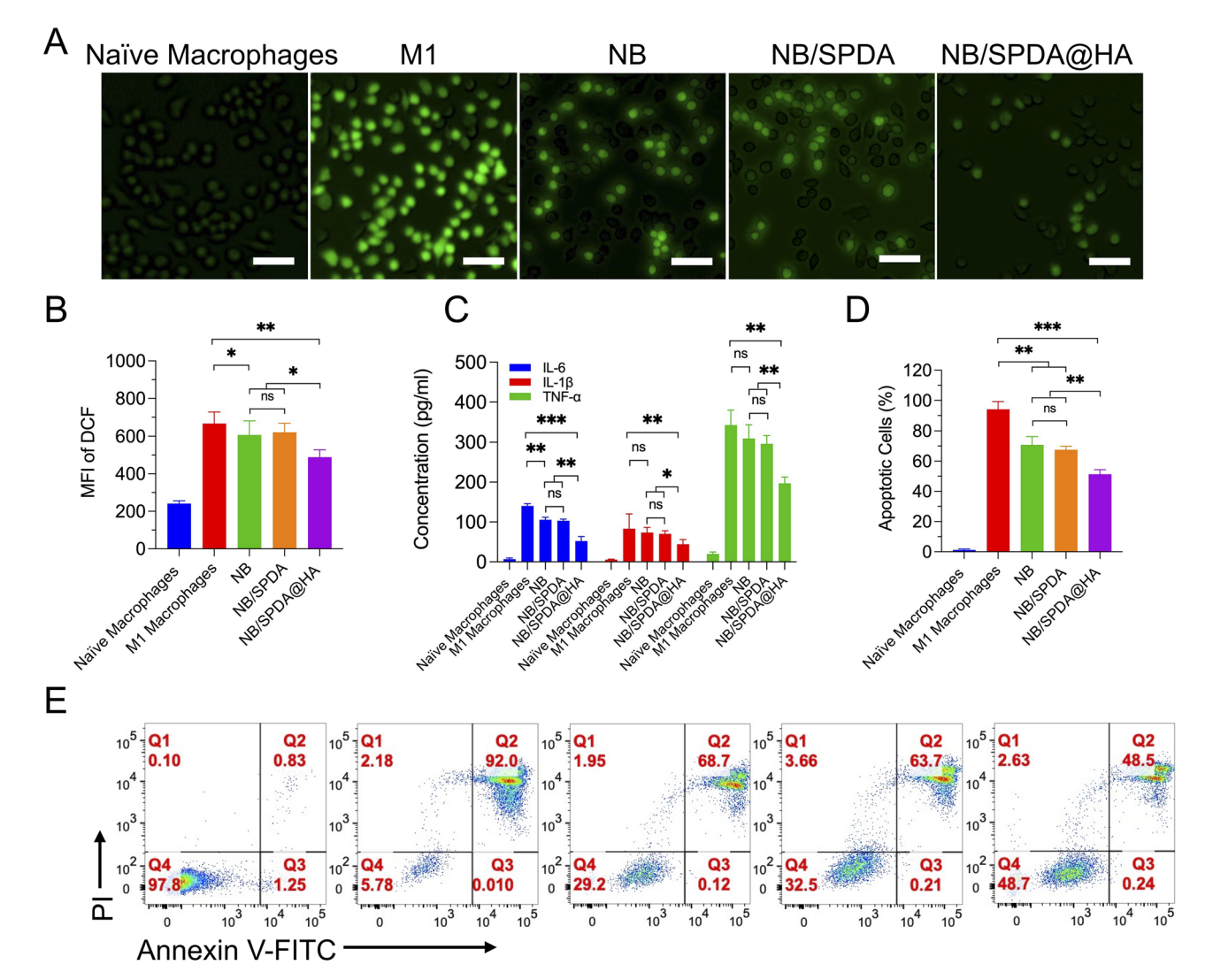


Fig. 4 Anti-inflammatory effects of NB/SPDA@HA nanoparticles. (A) Representative fluorescent images of fluorogenic probe DCF staining for detection of intracellular ROS generation. (B) FACS analysis of the fluorogenic probe DCF to quantify intracellular ROS generation after different treatments. (C) Quantitation of inflammatory cytokines secreted by RAW264.7 cells. (D) FACS analysis of RAW264.7 cell apoptosis. (E) Representative FACS plots for analysis of RAW264.7 cell apoptosis. Data is presented as mean \pm SD of three independent experiments (A–E). MFI, mean fluorescence intensity; ns, not significant; *p < 0.05; **p < 0.01; ***p < 0.001

As expected, LPS/IFN-γ stimulation induced production of inflammatory cytokines, including interleukin-6 (IL-6), interleukin-1 β (IL-1 β) and tumor necrosis factor (TNF- α) in macrophages (Fig. 4C). Similar to ROS, cytokine production was substantially inhibited by NB/SPDA@HA. Free NB and NB/SPDA also reduced IL-6 production but much less potent. The stronger anti-inflammatory effects of NB/SPDA@HA might be attributed to their higher cellular uptake and consequently higher intracellular accumulation of NB. Quantitation of intracellular NB would help to confirm the improvement in NB delivery by SPDA@HA nanoparticles, however, direct measurement of intracellular NB is technically challenging. 42 Since ROS are key signaling molecules and mediators of the inflammatory response,43 this result suggests that NB/SPDA@HA may alleviate inflammation by suppressing ROS production. In fact, NB has been reported to exert potent anti-inflammatory effects by inhibiting NLRP3 inflammasome activation in vascular

remodeling44 and cardiac stress.45 Moreover, NB has been shown to reduce cytokine production by inhibiting NF-κB and MAPK signaling pathways in liver injury. 46 Therefore, the potent anti-inflammatory property of NB/SPDA@HA is desirable to alleviate plaque progression and increase plaque stability, which may ultimately reduce the risk of acute coronary syndrome and stoke posed by atherosclerotic lesions. 47

Macrophage apoptosis causes development of the necrotic core which renders plaques vulnerable to rupture and acute lumenal thrombosis in advanced atherosclerotic lesions. 48 We therefore examined the influence of NB/SPDA@HA on macrophage apoptosis induced by LPS/IFN- γ treatment (Fig. 4D). As revealed by FACS analysis, NB/SPDA@HA significantly inhibited apoptosis (Fig. 4D and E). As expected, free NB and NB/SPDA also reduced cell apoptosis but to a lesser extent. NB may exert anti-apoptotic effects by reducing intracellular ROS (Fig. 4A and B)49 and/or by increasing intracellular NO

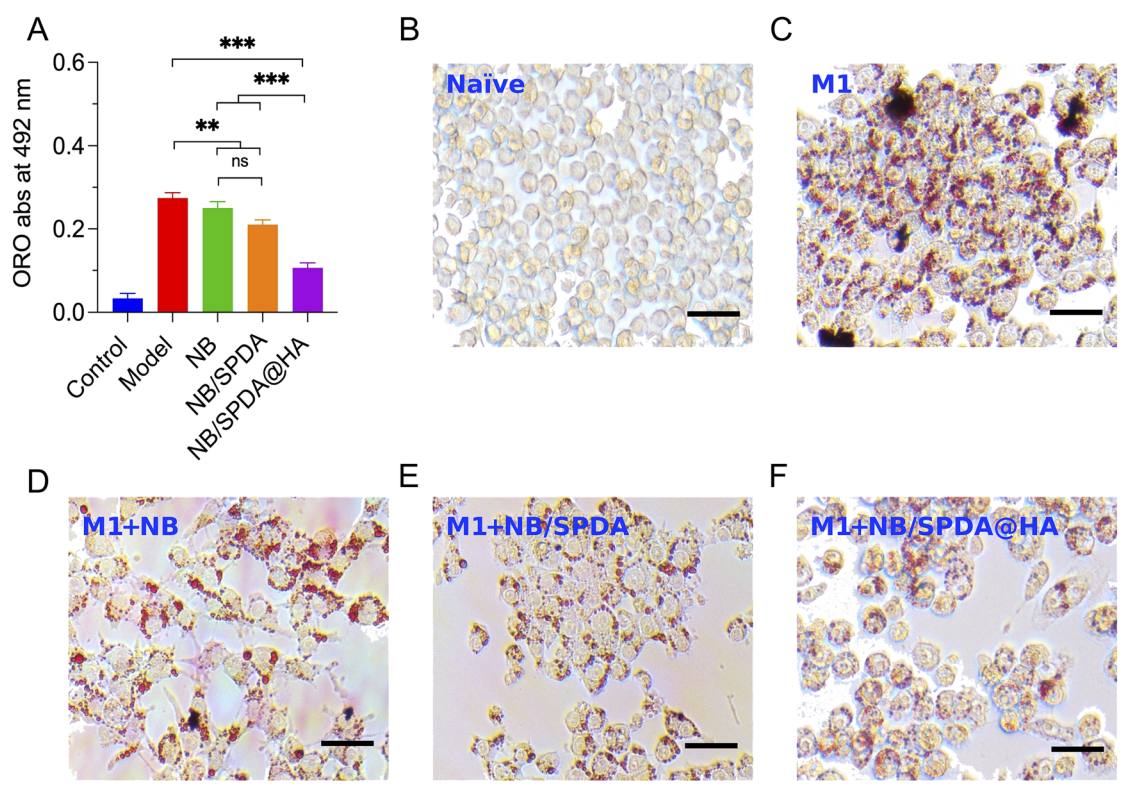


Fig. 5 Inhibition effects of foam cell formation. (A) Quantification of extracted contents of Oil Red O (ORO) in foam cells derived from M1 RAW264.7 macrophages after different treatments. Data is presented as mean \pm SD of three independent experiments. abs, absorption; ns, not significant; **p < 0.01; ***p < 0.001. (B) Representative ORO staining of naïve RAW264.7 macrophages. (C) Representative ORO staining of oxLDL-induced foam cells formatted by M1 RAW264.7 macrophages. (D-F) Representative ORO staining showing impacts of various treatments on foam cell formation by M1 RAW264.7 macrophages.

production.⁵⁰ Given the detrimental effects of macrophage apoptosis in advanced atherosclerosis,⁵¹ inhibition of apoptosis by NB/SPDA@HA is expected to promote plaque stabilization and reduce risk of cardiovascular disease.

NB/SPDA@HA inhibits foam cell formation

Macrophage foam cell formation amplifies inflammation and contributes to atherosclerosis initiation and progression. ^{51–53} To investigate if treatment with NB could suppress foam cell formation, we generated foam cells by incubating LPS/IFN-γ pre-treated RAW264.7 cells with oxidized low-density lipoprotein (oxLDL).9 As revealed by ORO staining, 48 h incubation with oxLDL induced accumulation of a large amount of lipids in the macrophages, indicating formation of foam cells (Fig. 5A-C). Such lipid accumulation was notably suppressed upon treatment with free NB, NB/SPDA or NB/SPDA@HA (Fig. 5D-F). To quantify intracellular lipid accumulation, ORO was extracted with isopropanol and its absorbance at 492 nm was measured. As shown in Fig. 5A, free NB, NB/SPDA and NB/SPDA@HA reduced intracellular lipid deposition by 8.76%, 23.36%, and 61.2%, respectively, compared with the model group with no treatment. More importantly, NB/SPDA@HA exerted the most pronounced inhibitory effects on foam cell formation among all the formulations. As ROS and inflammation are key drivers of foam cell formation,43,47 inhibition of oxLDL uptake by NB is

likely attributable to its antioxidative and anti-inflammatory activities. This is the first report, to our knowledge, that NB inhibits foam cell formation. This observation is clinically meaningful as accumulation of foam cells within arterial lining represents deterioration of atherosclerosis and NB is a beta blocker used for treatment of cardiovascular diseases.

Study limitations

While our study establishes the targeted delivery and therapeutic potential of NB/SPDA@HA nanoparticles *in vitro*, the absence of *in vivo* validation remains a key limitation. Future studies employing relevant atherosclerosis models, such as ApoE^{-/-} or LDLr^{-/-} mice, are necessary to confirm nanoparticle targeting and to rigorously assess anti-atherosclerotic efficacy and safety under physiological conditions. Such investigations will also yield critical insights into pharmacokinetics, biodistribution, plaque penetration, and long-term biocompatibility, which are essential for guiding translational development toward clinical applications.

Conclusions

In this study, CD44-targeted NB/SPDA@HA nanoparticles were developed for simultaneous diagnosis and treatment of atherosclerosis. The core formed with MSNs allowed NB loading

and subsequent surface functionalization with PDA polymer and HA to enable PAI imaging of atherosclerotic plaques and targeted drug delivery to lesional macrophages, respectively. Moreover, the silanols on the silica surface and the HAase in the plaque make the NB/SPDA@HA platform a dual-responsive drug release system in the context of atherosclerosis. NB/SPDA@HA nanoparticles exert potent activities in eliminating ROS, suppressing inflammation and cell apoptosis, and inhibiting foam cell formation *in vitro*. To conclude, we herein present a proof-of-concept for an innovative multifunctional plaque-targeting nanotheranostic platform, its efficacy and safety in atherosclerosis therapy warrant *in vivo* validation in future studies.

Author contributions

J. W. W. and K. C. Y. J. conceived and designed the study. Y. L. designed and performed majority of the experiments. B. P., C. H. and X. H. conducted experiments. Y. L., K. C. Y. J. and J. W. W. analyzed and interpreted the data and wrote the manuscript. All authors reviewed and edited the manuscript.

Conflicts of interest

There is no conflict of interest between the authors to declare.

Data availability

The data supporting this article have been included as part of the supplementary information (SI). Supplementary information is available: Fig. S1–S7 and Tables S1–S3. See DOI: https://doi.org/10.1039/d5na00497g.

Acknowledgements

This work was supported by the National University of Singapore (NUS) Cross-Faculty Grant (CFGFY20P14), the NUS Nano-NASH Program (NUHSRO/2020/002/NanoNash/LOA), the NUS Yong Loo Lin School of Medicine Nanomedicine Translational Research Program (NUHSRO/2021/034/TRP/09/Nanomedicine), the National Medical Research Council Centre Grant (NMRC CG21APR1008). Y.L. and C.H. would like to acknowledge the Ministry of Education research scholarship to support their graduate study at NUS. X.H. would like to thank the SINGA scholarship to support his graduate study at the NUS Yong Loo Lin School of Medicine.

References

- 1 https://www.who.int/health-topics/cardiovascular-diseases#tab=tab_1.
- 2 D. R. Owen, A. C. Lindsay, R. P. Choudhury and Z. A. Fayad, *Annu. Rev. Med.*, 2011, **62**, 25–40.
- 3 P. Schoenhagen, R. D. White, S. E. Nissen and E. M. Tuzcu, *Cleve. Clin. J. Med.*, 2003, **70**, 713–719.
- 4 J. Yu, H. N. Y. Nguyen, W. Steenbergen and K. Kim, *J. Nucl. Med.*, 2018, **59**, 1202–1207.

- 5 A. Negre-Salvayre, P. Guerby, S. Gayral, M. Laffargue and R. Salvayre, *Free Radic. Biol. Med.*, 2020, **149**, 8–22.
- 6 W. N. Nowak, J. Deng, X. Z. Ruan and Q. Xu, *Arterioscler. Thromb. Vasc. Biol.*, 2017, 37, e41–e52.
- 7 K. J. Bubb, G. R. Drummond and G. A. Figtree, *Cardiovasc. Res.*, 2020, **116**, 532–544.
- 8 D. R. Lewis, L. K. Petersen, A. W. York, S. Ahuja, H. Chae, L. B. Joseph, S. Rahimi, K. E. Uhrich, P. B. Haser and P. V. Moghe, *Cardiovasc. Res.*, 2016, **109**, 283–293.
- 9 S. Y. Chong, X. Wang, L. van Bloois, C. Huang, N. S. Syeda, S. Zhang, H. J. Ting, V. Nair, Y. Lin, C. K. L. Lou, A. A. Benetti, X. Yu, N. J. Y. Lim, M. S. Tan, H. Y. Lim, S. Y. Lim, C. H. Thiam, W. D. Looi, O. Zharkova, N. W. S. Chew, C. H. Ng, G. K. Bonney, M. Muthiah, X. Chen, G. Pastorin, A. M. Richards, V. Angeli, G. Storm and J. W. Wang, J. Contr. Release, 2023, 360, 344–364.
- 10 Y. Lin, J. Liu, S. Y. Chong, H. J. Ting, X. Tang, L. Yang, S. Zhang, X. Qi, P. Pei, Z. Yi, C. Huang, X. Hou, L. Gao, F. Torta, X. Liu, B. Liu, J. C. Y. Kah and J. W. Wang, *Small*, 2024, 20, e2401659.
- Y. Wang, L. Li, W. Zhao, Y. Dou, H. An, H. Tao, X. Xu, Y. Jia,
 S. Lu, J. Zhang and H. Hu, ACS Nano, 2018, 12, 8943–8960.
- 12 A. Zia, Y. Wu, T. Nguyen, X. Wang, K. Peter and H. T. Ta, *Cardiovasc. Res.*, 2020, **116**, 2055–2068.
- 13 Z. Li, J. C. Barnes, A. Bosoy, J. F. Stoddart and J. I. Zink, *Chem. Soc. Rev.*, 2012, **41**, 2590–2605.
- 14 C. Moore, F. Chen, J. Wang and J. V. Jokerst, *Adv. Drug Deliv. Rev.*, 2019, **144**, 78–89.
- 15 T. J. Beldman, M. L. Senders, A. Alaarg, C. Perez-Medina, J. Tang, Y. Zhao, F. Fay, J. Deichmoller, B. Born, E. Desclos, N. N. van der Wel, R. A. Hoebe, F. Kohen, E. Kartvelishvily, M. Neeman, T. Reiner, C. Calcagno, Z. A. Fayad, M. P. J. de Winther, E. Lutgens, W. J. M. Mulder and E. Kluza, ACS Nano, 2017, 11, 5785–5799.
- 16 C. A. Cuff, D. Kothapalli, I. Azonobi, S. Chun, Y. Zhang, R. Belkin, C. Yeh, A. Secreto, R. K. Assoian, D. J. Rader and E. Pure, J. Clin. Invest., 2001, 108, 1031–1040.
- 17 D. Hagg, S. Sjoberg, L. M. Hulten, B. Fagerberg, O. Wiklund, A. Rosengren, L. M. Carlsson, J. Boren, P. A. Svensson and A. Krettek, *Atherosclerosis*, 2007, 190, 291–297.
- 18 A. V. Poznyak, A. V. Grechko, V. A. Orekhova, V. Khotina, E. A. Ivanova and A. N. Orekhov, *Biomedicines*, 2020, **8**.
- 19 H. Mollnau, E. Schulz, A. Daiber, S. Baldus, M. Oelze, M. August, M. Wendt, U. Walter, C. Geiger, R. Agrawal, A. L. Kleschyov, T. Meinertz and T. Munzel, *Arterioscler. Thromb. Vasc. Biol.*, 2003, 23, 615–621.
- 20 M. Oelze, A. Daiber, R. P. Brandes, M. Hortmann, P. Wenzel, U. Hink, E. Schulz, H. Mollnau, A. von Sandersleben, A. L. Kleschyov, A. Mulsch, H. Li, U. Forstermann and T. Munzel, *Hypertension*, 2006, 48, 677–684.
- 21 P. T. Bot, G. Pasterkamp, M. J. Goumans, C. Strijder, F. L. Moll, J. P. de Vries, S. T. Pals, D. P. de Kleijn, J. J. Piek and I. E. Hoefer, *Eur. J. Clin. Invest.*, 2010, **40**, 818–827.
- 22 K. Oorni, K. Rajamaki, S. D. Nguyen, K. Lahdesmaki, R. Plihtari, M. Lee-Rueckert and P. T. Kovanen, *J. Lipid Res.*, 2015, 56, 203–214.

- 39 D. Pedicino, R. Vinci, A. F. Giglio, E. Pisano, I. Porto, R. Vergallo, G. Russo, A. Ruggio, A. D'Aiello, D. Flego, G. Annibali, F. Trotta, R. Piacentini, G. Niccoli, G. Liuzzo and F. Crea, J. Am. Coll. Cardiol., 2018, 72, 1490–1503.
- S. Wang, *Mater. Sci. Eng., C*, 2019, **105**, 110103. 24 K. W. Stahlfeld and E. L. Belmont, *Langmuir*, 2023, **39**, 8814–

23 W. Lei, C. Sun, T. Jiang, Y. Gao, Y. Yang, Q. Zhao and

- 8823. 25 Y. Gao and P. M. Vanhoutte, *J. Cardiovasc. Pharmacol.*, 2012,
- 59, 16–21.
- 26 M. Vrablik, A. Corsini and E. Tumova, *Curr. Atheroscler. Rep.*, 2022, 24, 161–169.
- 27 H. Lee, J. Rho and P. B. Messersmith, Adv. Mater., 2009, 21, 431–434.
- 28 B. Poinard, S. Kamaluddin, A. Q. Q. Tan, K. G. Neoh and J. C. Y. Kah, ACS Appl. Mater. Interfaces, 2019, 11, 4777–4789.
- 29 B. Poinard, S. A. E. Lam, K. G. Neoh and J. C. Y. Kah, *J. Contr. Release*, 2019, 300, 161–173.
- 30 S. Tiwari and P. Bahadur, Int. J. Biol. Macromol., 2019, 121, 556-571.
- 31 L. Feng, M. Cao, X. Ma, Y. Zhu and C. Hu, *J. Hazard. Mater.*, 2012, 217–218, 439–446.
- 32 Y. Liu, K. Ai, J. Liu, M. Deng, Y. He and L. Lu, *Adv. Mater.*, 2013, 25, 1353–1359.
- 33 U. Jana, A. K. Mohanty, P. K. Manna and G. P. Mohanta, *Colloids Surf. B Biointerfaces*, 2014, 113, 269–275.
- 34 L. A. Solovyov, O. V. Belousov, R. E. Dinnebier, A. N. Shmakov and S. D. Kirik, *J. Phys. Chem. B*, 2005, **109**, 3233–3237.
- 35 Y. Z. Zhou, Y. Cao, W. Liu, C. H. Chu and Q. L. Li, *ACS Appl. Mater. Interfaces*, 2012, 4, 6901–6910.
- 36 M. Sulpizi, M. P. Gaigeot and M. Sprik, J. Chem. Theory Comput., 2012, 8, 1037–1047.
- 37 N. Cheraga, Z. Ye, M.-J. Xu, L. Zou, N.-C. Sun, Y. Hang, C.-J. Shan, Z.-Z. Yang, L.-J. Chen and N.-P. Huang, *Nanoscale*, 2022, 14, 8709–8726.
- 38 Q. Zhao, H. Geng, Y. Wang, Y. Gao, J. Huang, Y. Wang, J. Zhang and S. Wang, ACS Appl. Mater. Interfaces, 2014, 6, 20290–20299.

- 40 B. Yameen, W. I. Choi, C. Vilos, A. Swami, J. Shi and O. C. Farokhzad, *J. Contr. Release*, 2014, **190**, 485–499.
- 41 E. Eruslanov and S. Kusmartsev, *Methods Mol. Biol.*, 2010, **594**, 57–72.
- 42 K. A. Abdullah, A. F. Qader, R. A. Omer, R. O. Kareem and M. I. Salih, *Discover Chem. Eng.*, 2025, 2, 136.
- 43 S. J. Forrester, D. S. Kikuchi, M. S. Hernandes, Q. Xu and K. K. Griendling, *Circ. Res.*, 2018, 122, 877–902.
- 44 J. Gao, Q. Xie, T. Wei, C. Huang, W. Zhou and W. Shen, *J. Cardiovasc. Pharmacol.*, 2019, 73, 326–333.
- 45 Q. Xie, T. Wei, C. Huang, P. Liu, M. Sun, W. Shen and P. Gao, *Sci. Rep.*, 2016, **6**, 34326.
- 46 R. T. B. Sabra, A. A. Bekhit, N. T. Sabra, N. A. A. El-Moeze and M. Fathy, *Stresses*, 2024, 4, 800–815.
- 47 P. Libby, P. M. Ridker and A. Maseri, *Circulation*, 2002, **105**, 1135–1143.
- 48 L. Gonzalez and B. L. Trigatti, *Can. J. Cardiol.*, 2017, **33**, 303–312
- 49 H. U. Simon, A. Haj-Yehia and F. Levi-Schaffer, *Apoptosis*, 2000. 5. 415–418.
- 50 G. Mercanoglu, N. Safran, M. Gungor, B. Pamukcu, H. Uzun, C. Sezgin, F. Mercanoglu and F. Fici, *Circ. J.*, 2008, 72, 660–670
- 51 S. Fang, S. Sun, H. Cai, X. Zou, S. Wang, X. Hao, X. Wan, J. Tian, Z. Li, Z. He, W. Huang, C. Liang, Z. Zhang, L. Yang, J. Tian, B. Yu and B. Sun, *Theranostics*, 2021, 11, 9358–9375.
- 52 A. Ajoolabady, D. Pratico, L. Lin, C. S. Mantzoros, S. Bahijri, J. Tuomilehto and J. Ren, *Cell Death Dis.*, 2024, **15**, 817.
- 53 M. Back, A. Yurdagul, I. Tabas, K. Oorni and P. T. Kovanen, *Nat. Rev. Cardiol.*, 2019, **16**, 389–406.